

Flexible strain sensors with high performance based on metallic glass thin film

H. J. Xian,^{1,2} C. R. Cao,^{1,2} J. A. Shi,^{1,2} X. S. Zhu,^{1,2} Y. C. Hu,^{1,2} Y. F. Huang,^{1,2} S. Meng,^{1,2} L. Gu,^{1,2} Y. H. Liu,^{1,2} H. Y. Bai,^{1,2} and W. H. Wang^{1,2,a)}

¹Institute of Physics, Chinese Academy of Sciences, Beijing 100190, China

²University of Chinese Academy of Sciences, Beijing 100049, China

(Received 29 June 2017; accepted 11 September 2017; published online 21 September 2017)

Searching strain sensitive materials for electronic skin is of crucial significance because of the restrictions of current materials such as poor electrical conductivity, large energy consumption, complex manufacturing process, and high cost. Here, we report a flexible strain sensor based on the $Zr_{55}Cu_{30}Ni_5Al_{10}$ metallic glass thin film which we name metallic glass skin. The metallic glass skin, synthesized by ion beam deposition, exhibits piezoresistance effects with a gauge factor of around 2.86, a large detectable strain range ($\sim 1\%$ or 180° bending angle), and good conductivity. Compared to other e-skin materials, the temperature coefficient of resistance of the metallic glass skin is extremely low ($9.04 \times 10^{-6} K^{-1}$), which is essential for the reduction in thermal drift. In addition, the metallic glass skin exhibits distinct antibacterial behavior desired for medical applications, also excellent reproducibility and repeatability (over 1000 times), nearly perfect linearity, low manufacturing cost, and negligible energy consumption, all of which are required for electronic skin for practical applications. *Published by AIP Publishing.* [<http://dx.doi.org/10.1063/1.4993560>]

The pace to pursuit electronic skin (e-skin) has never stopped since it has widespread applications in intelligent robots, biomimetic prosthetics, health monitoring, and other areas.^{1–9} Typically, e-skin consists of integrated flexible strain sensors so that external stimuli can be sensed.¹⁰ The exploration of e-skin includes four aspects: materials, devices, signal processing, and applications.¹¹ In the past, a wide variety of materials have been employed as strain sensitive materials for e-skin, such as carbon nanotubes, graphene, metal and semiconducting nanowires, metal nanoparticles, and organic and polymer-based materials.^{12–16} However, there exist deficiencies in these materials that prevent them from practical applications. For example, graphene synthesized via chemical vapor deposition is usually doped with defects or contaminants and cannot be directly grown on flexible substrates due to the high synthesis temperature beyond which the substrate cannot sustain;^{13,17} Metal nanoparticles, usually based on noble metals, exhibit dramatically increased electrical resistance in comparison with their bulk states because of the tunneling barrier;^{18–20} For nanowires, the fabrication costs are high, while the manufacturing scalability is low; Although the mechanical properties of organic and polymer materials are comparable to those of human skin, their poor conductivity makes operating voltage too high to be safe for portable devices and also results in extra energy consumption.^{1,21} Therefore, there is a great demand for e-skin materials that combine conductivity, mechanical flexibility, sensitivity, stability, manufacturing scalability low cost, and energy consumption for practical applications.

Metals and alloys are some of the oldest and most widely used materials but suffer from a small elastic limit that makes them uncompetitive when being applied to e-skin. Unlike conventional crystalline alloys, metallic glasses (MGs) are

alloys with disordered atomic structures and exhibit excellent mechanical properties including larger elastic limit, higher strength, better corrosion and wear resistance compared to their crystalline counterparts.²² Recently, the $Pd_{40}Cu_{30}Ni_{10}P_{20}$ metallic glass fiber has been reported to show an obvious^{23,24} piezoresistance effect with a gauge factor of 2.28. This suggests that MGs may be used to convert tactile stimuli into electronic signals. When being used in e-skin, piezoresistive strain sensors have several advantages, including rapid response, convenient signal transformation, low cost fabrication, etc.¹⁸ However, metallic glassy fibers are difficult to be integrated into ordered macro-scale arrays.

In this letter, we report a flexible sensor based on a metallic glass thin film (MGTF), specifically a $Zr_{55}Cu_{30}Ni_5Al_{10}$ “metallic glass skin (MG skin)” achieved by deposition of MGTF on a flexible polycarbonate substrate. The piezoresistance study indicates that the MGTF has a higher gauge factor (2.86) and a much larger elastic limit ($\sim 1\%$) than crystalline alloys, while the excellent conductivity and linear relationship between resistance change and applied strain still remain. In addition, the MG skin, which can be fabricated from a few mm^2 to more than $150 cm^2$, has an extremely low temperature coefficient of resistance ($9.04 \times 10^{-6} K^{-1}$), antimicrobial properties, etc. Combination of these properties makes MGTF a promising strain sensitive material for e-skin applications.

The MG skin was obtained by depositing $Zr_{55}Cu_{30}Ni_5Al_{10}$ MGTF on the polycarbonate substrate using an ion beam sputtering system. The piezoresistance effect, defined as the change in electrical resistance with applied strain, was investigated by four-probe resistance measurements. The antibacterial behavior was characterized by enumerating *Escherichia coli* (E. coli). Details about the experimental setup and the measurement process can be found in the [supplementary material](#).

Figure 1(a) shows the appearance of the flexible MGTF with a thickness of about 300 nm. The area of the MGTF is

^{a)}Authors to whom correspondence should be addressed: whw@iphy.ac.cn

25 cm², and the lateral dimensions of the samples vary from a few mm² to more than 150 cm² depending on the area of the substrate. The MGTF can be easily bent to an angle approaching 180°, demonstrating its excellent flexibility. High-resolution transmission electron microscopy (HRTEM) and glancing incidence X-ray diffraction (GIXRD) were employed to investigate the structure of the MGTF. As shown in Fig. 1(b), the maze-like patterns of HRTEM, the diffraction halo of the selected area electron diffraction (SAED), and the broad diffused scattering peak at $2\theta = 38^\circ$ in accordance with other Zr-based metallic glass patterns²⁵ all demonstrate the amorphous state of the sample. The thickness of the MGTF is controlled by the deposition time. With the decreasing thickness, more light can pass through the film in an exponential way. The transmittance spectra of MGTFs of different thicknesses are displayed in Fig. 1(d). When the thickness decreases to 10 nm, one can see that the MGTF appears to be transparent, as shown in Fig. 1(c).

Figure 2(a) presents the change in resistance $\Delta R/R_0$ (ΔR and R_0 are the change in resistance and initial resistance, respectively) as a function of strain applied on the MGTF. It can be seen that upon bending, the resistance increases linearly with increasing strain. The gauge factor (GF), which quantifies the sensitivity of the MGTF, can be estimated by²⁶

$$GF = \frac{R - R_0}{\varepsilon R_0}, \quad (1)$$

where ε is the equivalent strain upon bending. Linear fitting to the data indicates that the gauge factor is 2.86. This value is about 25% larger than that of previously reported metallic glassy fibers (2.28).²⁴ The elastic limit of the MG skin is about 1%, which is about ten times larger than that of conventional metals. Actually, when the strain is $\sim 1\%$, the bending angle θ exceeds 180° for the MG skin (Fig. S1, supplementary material). The I-V curve at a strain of 0.5% is shown in the inset of Fig. 2(a). The linearity indicates that the resistance of the MG skin does not change with current.

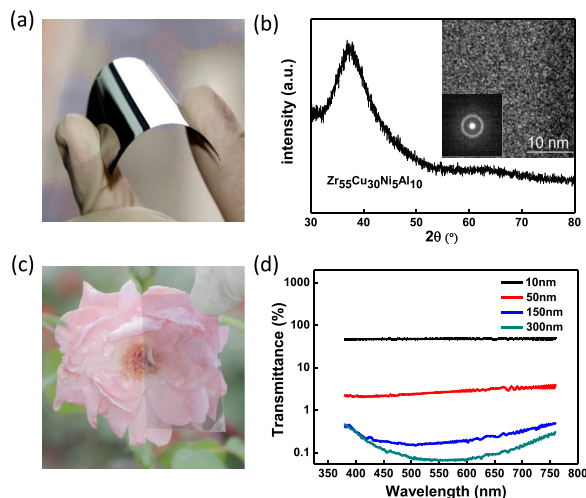


FIG. 1. (a) The image of the MG skin. (b) GIXRD pattern of the $Zr_{55}Cu_{30}Ni_5Al_{10}$ thin film. θ , XRD scattering angle; a.u., arbitrary units. Inset: HRTEM images and SAED patterns confirm its glassy nature. (c) Optical image illustrates that MG skin can be transparent. (d) Transmittance spectra of MGTF with different thicknesses (deposition time) in the wavelength range of 380–760 nm. The value for MGTF with 10 nm is about 54%.

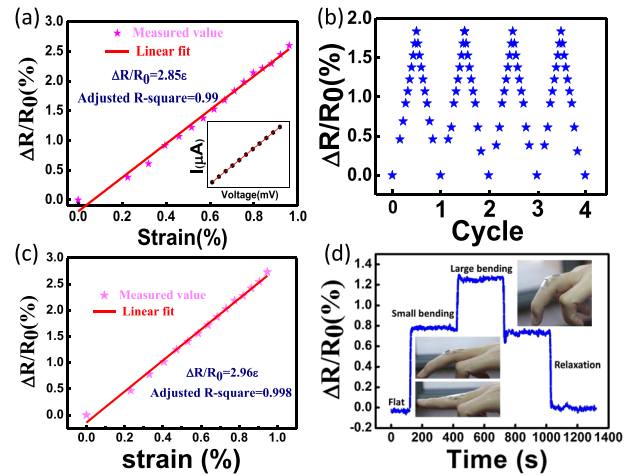


FIG. 2. Piezoresistance effect measurements of the MG thin films. (a) Relative change of resistance vs. strain; the inset shows the I-V curve of the sample. (b) Electrical resistance changes during the cycling test. (c) The relationship between the resistance change and the applied strain after bending 1000 times. (d) Diagram illustrating MG skin used to monitor movements of hands at different bending degrees.

Therefore, MGTF can be used in a wide range of currents and voltages. The MGTF has been tested for multiple operation cycles to ensure its stability, and the result is shown in Fig. 2(b). Upon unloading, $\Delta R/R_0$ decreases along the initial linear relationship and finally reduces to zero. No obvious hysteresis loop can be found within the accuracy of the equipment, illustrating its robustness and reproducibility. Even after being bent more than 1000 times, as shown in Fig. 2(c), the relationship between $\Delta R/R_0$ and strain remains linear. In addition, the deviation of the gauge factor from its initial value is negligible (less than 4%), indicating the reliability of the MGTF for e-skin application. From Fig. 2(c), we can also see that the minimum strain interval is less than 0.04%, suggesting its application for small strain measurements. The MG skin can detect human movement. For example, we stick the MG skin to the finger and the bending of the finger can be detected [Fig. 2(d)]. As shown, the bending degrees of the finger can be sensitively monitored by the MG skin, whose resistance exhibits a step-to-step behavior: a quick bending of the finger results in an immediate increase in the resistance to a higher stage; When the finger is relaxed, the resistance of the MG skin decreases instantaneously and rapidly returns to its initial value when the finger is completely stretched out. Although each posture during the monitoring was held for more than 200 s, significant burrs or fluctuations of the signal were absent, demonstrating potential applications of the MG skin in rehabilitation and bionics.

Since metallic glasses are in the metastable state, aging is their intrinsic behavior. Therefore, the stability of the MG skin is of concern. In order to evaluate the stability of the MG skin, we aged the MG skin in the air for ~ 100 days to inspect whether the aging could have an obvious impact on its function. As demonstrated in Fig. 3(a), we find that the gauge factor remains nearly constant with aging time. In addition, the deposition rate and the thickness of the MG skin contribute little to the change in the gauge factor [Fig. 3(c)], indicating that the value is intrinsic to the MG skin.

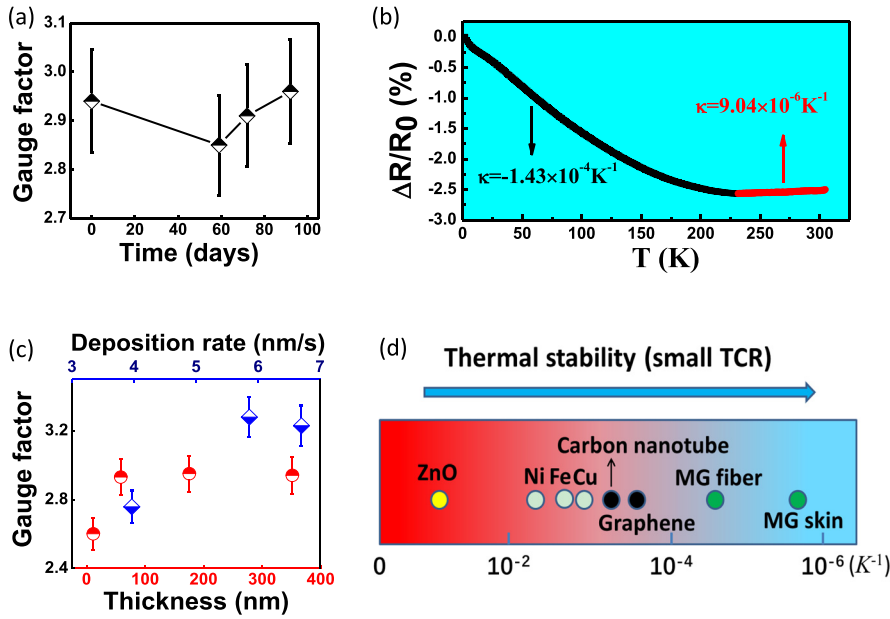


FIG. 3. (a) Gauge factor shows almost no change with aging time. (b) Dependence of relative changes of the electrical resistance on the temperature of the MG skin. (c) Dependence of sensitivity on the deposition rate and thickness of the sample. (d) Thermal stability of some conventional materials used for e-skin and MG skin. Smaller TCR stands for better thermal stability. The component of the metallic glass fiber is $\text{Pd}_{40}\text{Cu}_{30}\text{Ni}_{10}\text{P}_{20}$.

The excellent linearity of the piezoresistive response of the MGTF originates from its large geometrical contribution. For an isotropic conducting material such as metallic glass, the change in resistance can be written as²⁷

$$\frac{\Delta R}{R_0} = \frac{\Delta \rho}{\rho_0} + \frac{\Delta l}{l_0} - \frac{\Delta A}{A_0}, \quad (2)$$

where $\Delta \rho$, Δl , and ΔA and ρ_0 , l_0 , and A_0 stand for the change and original resistivity, length, and cross-sectional area of the sample, respectively. Taking $\nu = \Delta l/l_0$ and $\Delta A/A_0 = -2\nu\varepsilon$ into consideration, the gauge factor can be expressed as²⁷

$$GF = \frac{\Delta R}{\varepsilon R_0} = \frac{\Delta \rho}{\varepsilon \rho_0} + (1 + 2\nu), \quad (3)$$

where ν is Poisson's ratio of the conductor. The two terms on the right side of the equation characterize the contribution of resistivity and geometry changes to $\Delta R/R_0$.^{28–30} For $\text{Zr}_{55}\text{Cu}_{30}\text{Ni}_{15}\text{Al}_{10}$ metallic glass, Poisson's ratio is 0.376.³¹ This leads to a geometrical contribution of 61.7%. Compared to nickel (-8.1%) which has a giant but negative gauge coefficient and a nonlinear relationship between the resistance change and the applied strain, the geometrical contribution of MGTF is much larger.^{32,33} Therefore, it is reasonable that MG skin exhibits excellent linearity.

Because of its disordered structure, the resistance of MG is commonly larger than that of its crystalline counterpart.^{34,35} But the temperature coefficient of resistance (TCR) of MG is small owing to its insensitiveness to the details of the electronic structure and atomic arrangement.^{34,35} Figure 3(b) demonstrates the relationship between the resistance change and the temperature of the MG skin. With the increasing temperature, the resistance decreases, revealing a negative TCR of about $-1.43 \times 10^{-4} \text{K}^{-1}$. When the temperature reaches 231 K, the resistance tends to be constant irrespective of the temperature rise. The calculated TCR k is only $9.04 \times 10^{-6} \text{K}^{-1}$. The extremely low TCR is significant for electrical measurement instruments and microelectronic integrated circuits. Figure 3(d) compares the thermal stability

of resistance for different candidate materials in e-skin applications. One can see that MG skin exhibits 2–3 orders of magnitude smaller TCR than other metallic materials. Compared to graphene and carbon nanotubes (their TCR values are $-5 \times 10^{-4} \text{K}^{-1}$ and $-1.48 \times 10^{-3} \text{K}^{-1}$, respectively), which are popular for e-skin, the MG skin also exhibits superior thermal stability of resistance.^{36,37} For e-skin, the low TCR allows it to work in a wide temperature range, otherwise, extra bridges, strain foils, or crevices are needed to compensate the change in resistance caused by fluctuating temperature instead of strain.^{38,39} Also, the near dependence of resistance on temperature allows the integration of temperature sensors to fabricate multifunctional e-skin.

Figure 4(a) shows the result of antibacterial evaluation. After incubating *Escherichia coli* (*E. coli*) for 48 h, the ratios between *E. coli* and sample areas are $7.02 \times 10^5 \text{CFU/cm}^2$ and $2.6 \times 10^6 \text{CFU/cm}^2$ for MG skin and the polyethylene (PE) control plate, respectively. This indicates that the MG skin can prevent the growth of *E. coli*. The antibacterial rate of the MG skin, $\text{AR} = \frac{n_c - n_s}{n_c} \times 100\%$ (n_c and n_s are the numbers of viable colonies on the surface of PE and MG skin after incubation, respectively), is about 73%. We attribute the antimicrobial behavior to two factors: the surface physical properties of MG and release of metallic ions from MG. The surface topography of the MG skin investigated by atomic force microscopy is shown in Fig. 4(b). The root mean square roughness of the MG skin is only 0.358 nm, and the average peak-to-valley height is less than 2 nm, just about few atomic layers.⁴⁰ Moreover, the water contact angle (CA) between the water droplet and the MG skin, as presented in Fig. 4(c), is 90° , revealing the hydrophobicity of the MG skin. The surface smoothness and hydrophobicity make bacterial adhesion to the MG skin difficult so that fertilization and growth of bacteria are prevented at the surface.⁴¹ Another factor accounting for the antibacterial properties of the MG skin is the possible release of metallic ions from the MG skin, in particular, copper ions which can kill bacteria by damaging their cell walls and membranes.^{42,43}

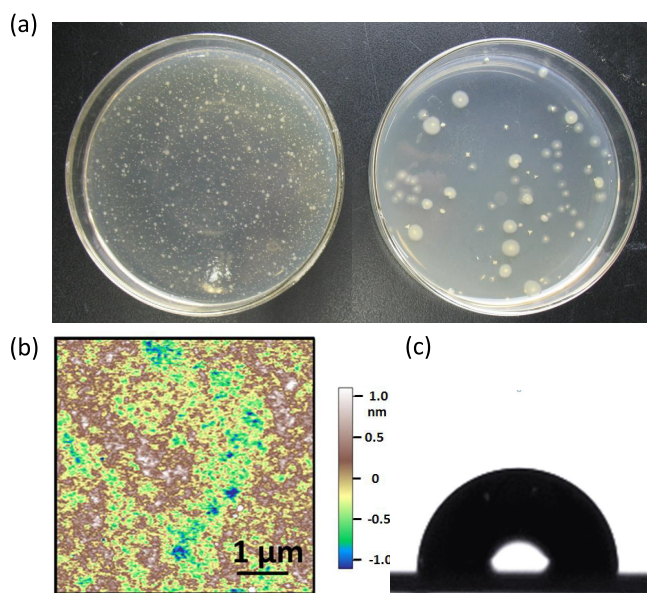


FIG. 4. (a) Optical images of *E. coli* on different materials after the antibacterial test. Left: PE control plate. Right: $Zr_{55}Cu_{30}Ni_5Al_{10}$ MG skin. (b) The AFM height image of MG skin. The rms roughness of the MG skin is 0.36 nm. (c) Image showing the water contact angle on the surface of MG skin.

Metallic strain sensors have been commercially used for many years due to their excellent electrical conductivity, linearity of resistance change with strain, and low cost. However, the available strain is less than 0.5% for most metallic materials,²⁵ which limits metals to be used in e-skin. For metallic glasses, one of the impressive advantages is their intrinsically high elastic limit $\sim 2\%$.⁴⁴ The elastic limits of MG can be further improved by reducing the dimension of MG.^{45–47} For example, the elastic limit of the $Zr_{55}Cu_{30}Ni_5Al_{10}$ thin film at room temperature (~ 300 K) can reach 4.2%.⁴⁸ This value is even larger than that of some polymers used for e-skin such as Poly[2,5-bis(3-alkylthiophen-2-yl)thieno(3,2-b)thiophene] (PBTTT) whose yield strain is less than 3%.⁴⁹ The large elastic limit ensures MGTF as a promising material for e-skin.

Although some materials, such as carbon nanotubes, exhibit high gauge factors, their relationship between the resistance change and the strain is nonlinear or the linear region is limited ($\epsilon < 0.2\%$).⁵⁰ For MG skin, the resistances change versus strain shows excellent linearity, which makes the resistance-strain transition more convenient and accurate. It should be noted that MG skin is not based on islands or wrinkles, and the sensitivity is the intrinsic value of the material. Making e-skin with both good electric conductivity and transparency at high strain is challenging.⁴ Probably, this can be resolved by MG skin. With the decreasing deposition time, we can make thinner MGTF. When the thickness decreases to about 10 nm, the MG skin tends to be transparent and the gauge factor remains 2.6, as large as thicker films. Furthermore, the transparent MG skin shows an electrical conductivity of about 5×10^3 S cm^{-1} , much larger than the previously reported value of e-skin based on carbon nanotubes (2200 S cm^{-1}).⁴ Such an electric conducting performance is better than that of the most majority of materials for e-skin. In our piezoresistance effect test, the voltage

applied to operate the device is less than 1 mV, which is completely safe for the human body.^{21,51} The low power consumption of about 10^{-7} W makes the MG skin beneficial for energy conservation and the endurance of the device. In addition, the antimicrobial properties of the MG skin are promising for medical equipment. Furthermore, the high strength, good corrosion, and wear resistance⁵² endow the MG skin effective protection from surrounding hazards.

In summary, we developed MG skin based on the piezoresistance effect of $Zr_{55}Cu_{30}Ni_5Al_{10}$ MGTF. The MG skin is fabricated by depositing MGTF on a flexible substrate. Through controlling the deposition time and thus the thickness, the MG skins exhibit various light transmittances from 0.2% to 54%. The large area MG skin also exhibits good conductivity ($> 5 \times 10^3$ S cm^{-1}), high sensitivity ($GF \sim 2.86$), perfect linearity, large elastic limit ($> 1\%$), excellent stability and repeatability, extremely low TCR value (9.04×10^{-6} K $^{-1}$), little energy consumption (10^{-7} W), low cost and ease of fabrication, and distinct antimicrobial behavior. Glass forming alloys with various elements and wide forming composition ranges show different characteristics and properties. Thus, it is possible to continuously improve the performance of the MG skin by composition modification. Besides demonstrating a candidate material for e-skin, this work also provides an unprecedented perspective on the functional use of metallic glasses by combining their excellent electrical, mechanical, and thermal properties together.

See [supplementary material](#) for the complete experimental setup and measurement process.

We are grateful for experimental assistance from J. Zhao, C. Wang, L. Z. Zhao, P. Luo, D. Q. Zhao, and X. H. Cheng (Department of Physics, Jilin University). The financial support of the NSF of China (Grant Nos. 51571209 and 51461165101), the MOST 973 Program of China (No. 2015CB856800), and the Key Research Program of Frontier Sciences, CAS (QYZDY-SSW-JSC017) is appreciated.

¹M. L. Hammock, A. Chortos, B. C.-K. Tee, J. B.-H. Tok, and Z. N. Bao, *Adv. Mater.* **25**, 5997 (2013).

²B. C.-K. Tee, C. Wang, R. Allen, and Z. N. Bao, *Nat. Nanotechnol.* **7**, 825 (2012).

³C. Wang, D. Hwang, Z. B. Yu, K. Takei, J. Park, T. Chen, B. W. Ma, and A. Javey, *Nat. Mater.* **12**, 899 (2013).

⁴D. J. Lipomi, M. Vosgueritchian, B. C.-K. Tee, S. L. Hellstrom, J. A. Lee, C. H. Fox, and Z. N. Bao, *Nat. Nanotechnol.* **6**, 788 (2011).

⁵J. Park, Y. Lee, J. Hong, Y. Lee, M. Ha, Y. Jung, H. Lim, S. Y. Kim, and H. Ko, *ACS Nano* **8**, 12020 (2014).

⁶B.-U. Hwang, J.-H. Lee, T. Q. Trung, E. Roh, D.-I. Kim, S.-W. Kim, and N.-E. Lee, *ACS Nano* **9**, 8801 (2015).

⁷Z. L. Wang and J. Song, *Science* **312**, 242 (2006).

⁸C. C. Nunez, W. T. Navaraj, E. O. Polat, and R. Dahiya, *Adv. Funct. Mater.* **27**, 1606287 (2017).

⁹X. W. Wang, Y. Gu, Z. P. Xiong, Z. Cui, and T. Zhang, *Adv. Mater.* **26**, 1336 (2014).

¹⁰M. Segev-Bar, N. Bachar, Y. Wolf, B. Ukrainsky, L. Sarraf, and H. Haick, *Adv. Mater. Technol.* **2**, 1600206 (2017).

¹¹V. Lumelsky, M. S. Shur, and S. Wagner, *Sel. Top. Electron. Syst.* **18**, 28 (2000).

¹²I. Kang, M. J. Schulz, J. H. Kim, V. Shanovand, and D. L. Shi, *Smart. Mater. Struct.* **15**, 737 (2006).

¹³J. Zhao, G. L. Wang, R. Yang, X. B. Lu, M. Cheng, C. L. He, G. B. Xie, J. L. Meng, D. X. Shi, and G. Y. Zhang, *ACS Nano* **9**, 1622 (2015).

- ¹⁴Y. Wang, A. Wang, T. T. Yang, X. Li, X. B. Zang, M. Zhu, K. Wang, D. Wu, and H. W. Zhu, *Adv. Funct. Mater.* **24**, 4666 (2014).
- ¹⁵K. Takei, T. Takahashi, J. C. Ho, H. Ko, A. G. Gillies, P. W. Leu, R. S. Fearing, and A. Javey, *Nat. Mater.* **9**, 821 (2010).
- ¹⁶S. Nambiar and J. T. W. Yeow, *Biosens. Bioelectron.* **26**, 1825 (2011).
- ¹⁷A. Pirkle, J. Chan, A. Venugopal, D. Hinojos, C. W. Magnuson, S. McDonnell, L. Colombo, E. M. Voge, R. S. Ruoff, and R. M. Wallace, *Appl. Phys. Lett.* **99**, 122108 (2011).
- ¹⁸D. Lee, H. Lee, Y. J. Jeong, Y. Ahn, G. Nam, and Y. Lee, *Adv. Mater.* **28**, 9364 (2016).
- ¹⁹K. Takei, Z. B. Yu, M. Zheng, H. Ota, T. Takahashi, and A. Javey, *Proc. Natl. Acad. Sci. U. S. A.* **111**, 1703 (2014).
- ²⁰M. Segev-Bar, G. Konvalina, and H. Haick, *Adv. Mater.* **27**, 1779 (2015).
- ²¹S. Bauer and M. Kaltenbrunner, *Nature* **539**, 365 (2016).
- ²²W. H. Wang, *Adv. Mater.* **21**, 4524 (2009).
- ²³J. Yi, X. X. Xia, D. Q. Zhao, M. X. Pan, H. Y. Bai, and W. H. Wang, *Adv. Eng. Mater.* **12**, 1117 (2010).
- ²⁴J. Yi, H. Y. Bai, D. Q. Zhao, M. X. Pan, and W. H. Wang, *Appl. Phys. Lett.* **98**, 241917 (2011).
- ²⁵J. C. Oh, T. Ohkubo, Y. C. Kim, E. Fleury, and K. Hono, *Scr. Mater.* **53**, 165 (2005).
- ²⁶G. R. Higson, *J. Sci. Instrum.* **41**, 405 (1964).
- ²⁷C. Grimaldi, P. Ryser, and S. Strässler, *Phys. Rev. B.* **64**, 064201 (2001).
- ²⁸M. L. Meyer, *J. Strain. Anal. Eng. Des.* **2**, 324 (1967).
- ²⁹M. Allen, *Phys. Rev.* **52**, 1246 (1937).
- ³⁰C. S. Smith, *Phys. Rev.* **94**, 42 (1954).
- ³¹Y. Tong, Ph.D. thesis, The University of Tennessee, May 2015.
- ³²M. C. Martin, *J. Appl. Phys.* **41**, 5163 (1970).
- ³³E. Klokholm, *J. Vac. Sci. Technol.* **10**, 235 (1973).
- ³⁴C. Suryanarayana and A. Inoue, *Bulk Metallic Glasses* (CRC Press, 2010), p. 286.
- ³⁵M. A. Howson and B. L. Gallagher, *Phys. Rep.* **170**, 265 (1988).
- ³⁶P. A. Tipler and G. Mosca, *Physics for Scientists and Engineers* (Macmillan, 2007).
- ³⁷P. Z. Sun, M. Zhu, K. L. Wang, M. L. Zhong, J. Q. Wei, D. H. Wu, and H. W. Zhu, *ACS. Appl. Mater. Inter.* **5**, 9563 (2013).
- ³⁸Q. Wang, J. N. Ding, and W. X. Wang, *Sens. Actuators A: Phys.* **120**, 468 (2005).
- ³⁹L. Z. Yi, W. H. Jiao, C. M. Zhu, K. Wu, C. Zhang, L. H. Qian, S. Wang, Y. T. Jiang, and S. L. Yuan, *Nano. Res.* **9**, 1346 (2016).
- ⁴⁰Y. H. Liu, D. Wang, K. Nakajima, W. Zhang, A. Hirata, T. Nishi, A. Inoue, and M. W. Chen, *Phys. Rev. Lett.* **106**, 125504 (2011).
- ⁴¹P. T. Chiang, G. J. Chen, S. R. Jian, Y. H. Shih, J. S.-C. Jang, and C. H. Lai, *Fooyin. J. Health. Sci.* **2**, 12 (2010).
- ⁴²Y. H. Kim, Y.-R. Choi, K. M. Kim, and S. Y. Choi, *Appl. Surf. Sci.* **258**, 3823 (2012).
- ⁴³M. Wang and W. X. Wang, *Environ. Sci. Technol.* **42**, 940 (2008).
- ⁴⁴W. L. Johnson, *MRS Bull.* **24**, 42 (1999).
- ⁴⁵D. C. Jang and J. R. Greer, *Nat. Mater.* **9**, 215 (2010).
- ⁴⁶H. Bei, Z. P. Lu, and E. P. George, *Phys. Rev. Lett.* **93**, 125504 (2004).
- ⁴⁷T. Lin, Y. Q. Cheng, Z. W. Shan, J. Li, C. C. Wang, X. D. Han, J. Sun, and E. Ma, *Nat. Commun.* **3**, 609 (2012).
- ⁴⁸W. L. Johnson and K. Samwer, *Phys. Rev. Lett.* **95**, 195501 (2005).
- ⁴⁹B. O'Connor, E. P. Chan, C. Chan, B. R. Conrad, L. J. Richter, R. J. Kline, M. Heeney, I. McCulloch, C. L. Soles, and D. M. De Longchamp, *ACS. Nano* **4**, 7538 (2010).
- ⁵⁰J. Cao, Q. Wang, and H. J. Dai, *Phys. Rev. Lett.* **90**, 157601 (2003).
- ⁵¹J. Y. Oh, S. R. Gagne, Y. C. Chiu, A. Chortos, F. Lissel, G.-J. N. Wang, B. C. Schroeder, T. Kurosawa, J. Lopez, T. Katsumata, J. Xu, C. X. Zhu, X. D. Gu, W. G. Bae, Y. Kim, L. Jin, J. W. Chung, J. B.-H. Tok, and Z. N. Bao, *Nature* **539**, 411 (2016).
- ⁵²Q. Chen, L. Liu, and S. M. Zhang, *Front. Mater. Sci. China* **4**, 34 (2010).